Materials Research Proceedings 64 (2026) 692-699 https://doi.org/10.21741/9781644904091-86

Potassium-Deintercalated Birnessite ($Mn_7O_{13}\cdot 5H_2O$) as Cathode for Advanced Aqueous Zinc-Ion Batteries

Hamza AFARYATE[1,a*], Mohamed KERROUMI[1], Mehdi KARBAK[1], Bouchaib MANOUN[2], Youssef TAMRAOUI[1], Fouad GHAMOUSS[1,f*]

[1]College of Chemical Sciences and Engineering (CCSE), Department of Materials Science, Energy and Nano-engineering (MSN), Mohammed VI Polytechnic University (UM6P), Morocco

[2]University Hassan 1st, FST, Settat, Morocco

[a]hamza.afaryate@um6p.ma, [f]fouad.ghamouss@um6p.ma

Keywords: Zinc-Ion Batteries, Potassium-Birnessite, Cathode Materials, Acid Leaching, Aqueous Batteries

Abstract. Aqueous zinc-ion batteries (AZIBs) have gained increasing interest as a low-cost, intrinsically safe platform for grid energy-storage applications. Nevertheless, their development is hampered by sluggish Zn^{2+} diffusion and structural instability of cathodes, largely due to the large hydrated radius of Zn^{2+} ions. In this work, a hydrated birnessite-type manganese oxide, denoted L-KMO ($Mn_7O_{13}\cdot 5H_2O$), is synthesized via a mild acid-leaching strategy applied to potassium birnessite (KMO, $K_{0.37}MnO_2$). Structural and physicochemical characterizations confirm successful potassium removal and formation of a hydrated layered framework with expanded interlayer spacing. When evaluated as a cathode for AZIBs, L-KMO delivers a high capacity of up to 347 mAh g^{-1} at 50 mA g^{-1}, along with excellent Coulombic efficiency of approximately 96-100% and stable cycling behavior. This simple and scalable synthesis approach provides an effective route for tailoring manganese-oxide cathodes toward advanced AZIBs.

Introduction

Zinc-ion batteries have appeared as an attractive technology for grid energy storage, due to the abundance and low cost of zinc, along with its high theoretical capacity (820 mAh g^{-1}), its low redox potential (-0.762 V vs SHE), and intrinsic safety. The electrochemical performance of ZIBs, including operating voltage and reversible capacity, is primarily dictated by the nature of the cathode material, which controls zinc-ion storage behavior and reaction kinetics. Consequently, the development of advanced cathode materials remains the main challenge limiting further progress in high-performance ZIBs and their commercialization [1,2]. To date, various cathode systems such as manganese and vanadium oxides, metal-organic frameworks, and Prussian blue analogues have been investigated. Nevertheless, each class of these materials has specific shortcomings that affect practical implementation. Typical average working voltage is moderate for vanadium oxides, and they tend to dissolve into aqueous solutions, leading to reduced energy density and raising environmental concerns.[3,4] While MOFs have tunable porosity, they are typically characterized by low electronic conductivity due to the presence of insulating organic linkers. [4,5] The open framework of a Prussian blue analogue provides good kinetics, but moderate capacity compared to dense oxide cathodes. [1] Among these cathodes, manganese oxides appear to be the best candidate for commercial AZIB thinks to the structural diversity, which arises from the [MnO_6] octahedral connecting by edges and corners to form tunneled (Pyrolusite, Hollandite, Ramsdellite, Spinel…) and layered (δ) structures, giving them different valences and structural properties, low toxicity, natural abundance, high specific capacity, and relatively high working voltage, positioning them as key materials for the development of ZIB technologies.[6,7]

Content from this work may be used under the terms of the Creative Commons Attribution 3.0 license. Any further distribution of this work must maintain attribution to the author(s) and the title of the work, journal citation and DOI. Published under license by Materials Research Forum LLC.

Materials Research Proceedings 64 (2026) 692-699 https://doi.org/10.21741/9781644904091-86

Many strategies have been explored to mitigate the inherent limitations of cathodes made from manganese, including the incorporation of conductive carbon networks like carbon nanotubes or graphene, defect engineering techniques, and creating new advanced aqueous electrolytes (e.g., eutectic electrolytes, molecularly crowded electrolytes, water-in-salt electrolytes) that are compatible with Mn-based batteries [8-10]. However, many of the traditional post-treatment techniques provide limited advantages in terms of optimization. Also, recently, a technique of acid leaching has been found to be an efficient way to control the properties of Mn oxides through specific changes in chemical composition, phase transitions, and creation of defect structures while eliminating the need for any additional post-treatment steps. This strategy was employed to produce spinel-type Mn oxides with enhanced electrochemical performance by removing Li^+ and Zn^{2+} from $LiMn_2O_4$ and $ZnMn_2O_4$, respectively, while preserving the Mn framework, offering favorable ion-diffusion pathways. [11,13]

Among manganese oxides, layered birnessite (K_xMnO_2) is particularly attractive owing to its two-dimensional MnO_6 frameworks and accessible interlayer galleries. However, the crowded interlayers caused by the presence of potassium ions and the tendency of nanosheets to stick together impede Zn^{2+} diffusion, limiting the capacity and affecting the cycling stability. To address these limitations, we derive a layered manganese oxide $Mn_7O_{13}\cdot 5H_2O$ (L-KMO) from K-birnessite (KMO) by selectively deintercalating potassium via mild acid treatment. The resulting leached material was thoroughly characterized in terms of its structure and microstructure and subsequently evaluated as a cathode in AZIB, representing a previously unexplored application.

Material characterization

Materials synthesis

All reagents are ≥ 99% pure or of analytical grade. The chemicals were sourced from Sigma-Aldrich and employed as received. Double-distilled water was used in all experimental procedures. K-birnessite (KMO, $K_{0.37}MnO_2$) was prepared by a sol–gel route following literature protocols [14,15]. 3.0 g of $KMnO_4$ dissolved in 50 mL of double-distilled water and rapidly poured into 20 mL of an aqueous D(+)-glucose solution under vigorous stirring ($KMnO_4$: glucose molar ratio = 1:1.5), where glucose acted as a complexing/reducing agent. After solvent evaporation, the resulting brown gel was cooled to room temperature (RT), then oven-dried at 100 °C for 12 h to afford a xerogel, which was subsequently heat-treated in air at 400 °C for 2 h to yield the final oxide material.

To selectively remove interlayer K^+, 2.0 g of KMO was dispersed in 200 mL of 0.2 M HCl and stirred at RT for 12 h.[13] The suspension was centrifuged, and the solid was washed repeatedly with water to neutral pH, then vacuum dried.

Characterization methods

Crystalline structure of the sample was analyzed using Bruker AXS D8 Advance X-ray diffractometer. Raman spectra were recorded employing a LabRAM HR Evolution Raman microscope equipped with a 514 nm excitation laser over the range of 200-1000 cm^{-1}. Thermal properties were evaluated using a differential thermal analyzer (DTA, Henven) under a nitrogen atmosphere from 23 to 700 °C at a heating rate of 10 °C·min^{-1}. Sample morphology and elemental mapping were examined by a TESCAN VEGA3 scanning electron microscope (SEM). Rietveld refinement of the XRD data was conducted using WinPLOTR graphical interface of the FullProf software package. The refinement procedure involved sequential optimization of instrumental parameters, background, scale factor, and peak profile functions. Background contributions were fitted using a fifth-order polynomial, followed by refinement of the structural parameters.

Materials Research Proceedings 64 (2026) 692-699 https://doi.org/10.21741/9781644904091-86

Electrochemical measurements

CR2032 coin cells were employed to perform the electrochemical tests. Cathodes were fabricated by applying a slurry with a 7:2:1 weight ratio of L-KMO, Super P, and Polyvinylidene fluoride onto a titanium foil. The cells were put together using L-KMO cathode (mass loading ~ 2 $mg \cdot cm^{-2}$), a glass fiber-based separator, an aqueous electrolyte consisting of 3 M $ZnSO_4$ with 0.2 M Mn_2SO_4 solution, and Zn foil anode. To ensure the removal of dissolved oxygen from the electrolyte, argon gas was continuously purged through the solution for 20 minutes. The assembled coin cells were then evaluated using cyclic voltammetry (CV) and galvanostatic charge-discharge (GCPL) techniques on a BioLogic battery testing system, operated over a voltage window of 0.8-1.8 V vs Zn^{2+} /Zn.

Results and Discussion

Structural changes induced by the acid-leaching process were studied using X-ray diffraction (XRD), as presented in Fig. 1a. The pristine sample (KMO) was indexed to monoclinic potassium birnessite, $K_{0.37}MnO_2$ (PDF 96-432-4653), with C 1 2/m 1 space group (No. 12). Its stoichiometry was further confirmed by Rietveld refinement (Fig. 1b), which shows excellent agreement between the experimental and calculated profiles. After leaching, the diffraction pattern transformed into that of orthorhombic hydrated layered manganese oxide, $Mn_7O_{13} \cdot 5H_2O$ (PDF 00-023-1239), with Pbca space group (No. 61). Additionally, thermogravimetric analysis (Fig. 1c) displays two distinct dehydration steps. The first mass loss appeared at around 150 ^oC assigned to physisorbed water (~2 H_2O), while the second appeared at approximately 560 ^oC attributed to coordinated/structural water (~3 H_2O). The total mass loss (~13.18%) closely matches the theoretical (13.2 wt%) expected for five water molecules in the $Mn_7O_{13} \cdot 5H_2O$ structure, thereby confirming the presence of 5 H_2O per formula unit in the leached KMO.

Raman spectroscopy was also used to probe the structural modifications associated with K^+ extraction. Spectra of KMO and L-KMO were recorded over 200-1000 cm^{-1} (Fig. 1d). Consistent with prior literature reports, a prominent band was observed for KMO at 655 cm^{-1}, attributed to A_{1g} symmetric stretching of Mn-O in MnO_6 octahedra, where motion of oxygen atoms dominates.[16] After acid leaching, this band downshifts to 643 cm^{-1} in L-KMO, indicating structural distortion of the lattice and changes in the manganese-oxygen bond strengths and lengths arising from the removal of interlayer K^+. Additional modes below 600 cm^{-1} located at 373, 316, and 287 cm^{-1} in KMO spectra and associated with MnO_6 bending vibrations also shift to 358, 302, and 273 cm^{-1}, respectively, in L-KMO, further corroborating the structural relaxation accompanying potassium deintercalation. [17,18]

Materials Research Proceedings 64 (2026) 692-699 https://doi.org/10.21741/9781644904091-86

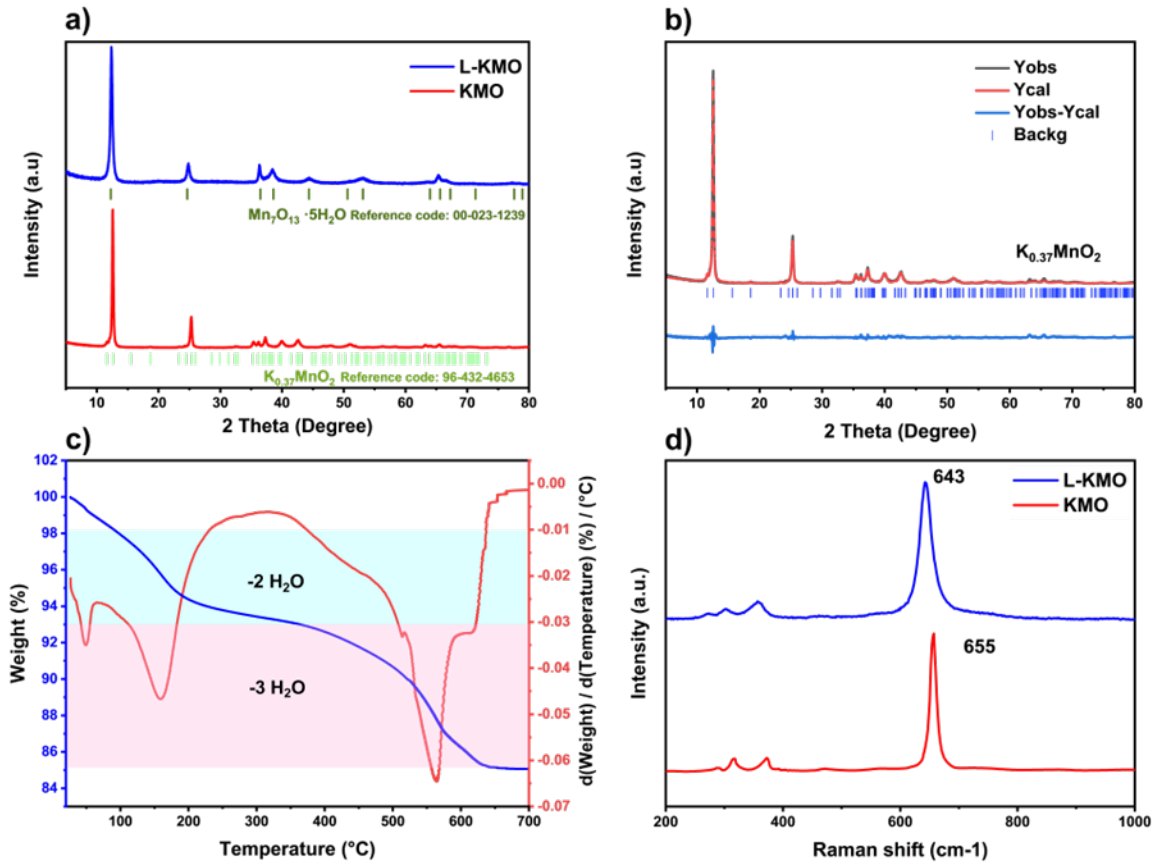


Fig. 1. *Structural and thermal characterization of KMO and L-KMO:* ***(a)*** *XRD patterns,* ***(b)*** *Rietveld refinement of KMO,* ***(c)*** *TGA/DTG of L-KMO, and* ***(d)*** *Raman spectra.*

Surface features of the synthesized KMO and L-KMO samples were investigated using scanning electron microscopy, as presented in Fig. 2. Result reveals that the pristine K-birnessite (KMO) forms porous agglomerates of stacked, plate-like nanocrystallites on the order of 5-20 µm. Following acid leaching, L-KMO shows cauliflower-like microclusters (~5-15 µm) composed of finer, granular/etched nanodomains and a higher degree of surface roughness and porosity. This morphological evolution increases accessible surface area and opens transport pathways, changes that are expected to facilitate Zn^{2+} insertion kinetics. Moreover, Elemental mapping via energy-dispersive X-ray spectroscopy further confirms the potassium extraction from KMO following the acid-leaching process, as demonstrated by the disappearance of the potassium element from mapping images.

Materials Research Proceedings 64 (2026) 692-699 https://doi.org/10.21741/9781644904091-86

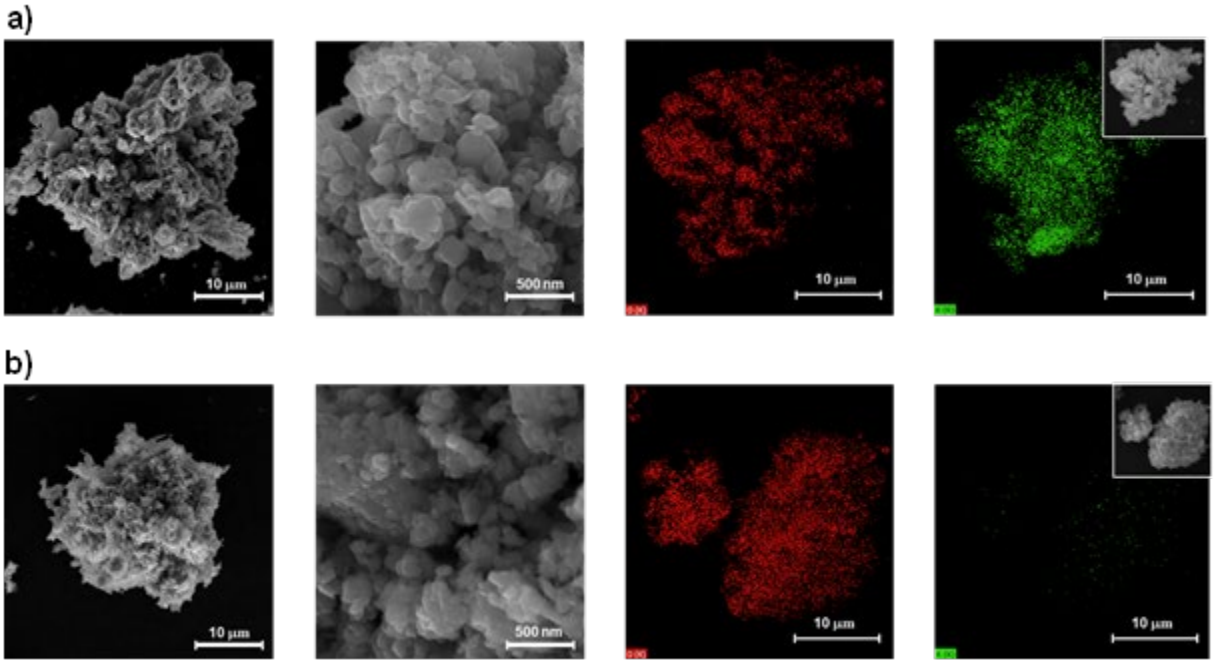


Fig. 2. SEM and elemental (Mn, K) mapping of (a) KMO, (b) L-KMO.

To assess the electrochemical performances of the synthesized L-KMO cathode in zinc-ion batteries, cyclic voltammetry measurements were first recorded under a scanning rate of 0.1 mV s^{-1} (Fig. 3a). CV curves exhibit two well-defined cathodic peaks at approximately 1.36 and 1.24 V, accompanied by corresponding anodic features around 1.61 and 1.66 V, characteristic of sequential H^+/Zn^{2+} co-insertion-extraction in manganese oxide hosts.[13] Furthermore, no activation cycle or phase transition was observed, as the cv curves retained the same behavior during the first cycles. Galvanostatic charge/discharge (GCD) measurements collected at 50 mA g^{-1} over the same potential window (Fig. 3b-c) display two discharge and two charge plateaus, consistent with the CV features and indicative of two dominant redox processes. L-KMO exhibits an initial reversible capacity of ~160 mAh g^{-1}, which gradually activates to reach ~347 mAh g^{-1} after 73 cycles, while retaining a high Coulombic efficiency (≈96-100%). This progressive capacity rise is attributed to the electrode activation process, resulting from a combination of enhanced electrolyte wettability, exposure of additional active sites, and the disruption of agglomerates during cycling due to the repeated insertion/extraction of ions.[19,20]

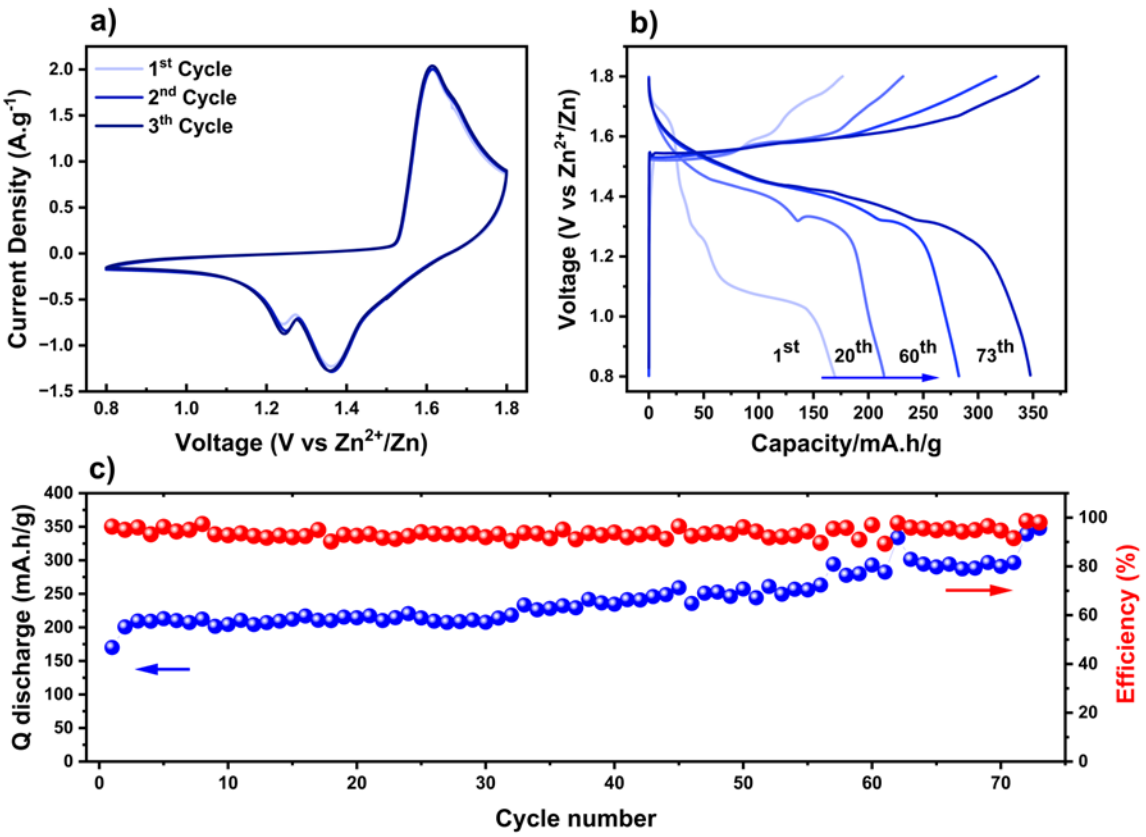


Fig. 3. (a) CV curves, (b) GCPL patterns, and (c) long-term cycling of L-KMO.

Conclusions

In this work, a layered hydrated manganese oxide (L-KMO, space group: Pbca) was produced through mild acid leaching of K-birnessite (KMO, $K_{0.37}MnO_2$, C 1 2/m 1) synthesized via a simple sol-gel process. XRD, Raman, EDX, and TGA analyses confirmed the synthesis of pure K-birnessite, followed by successful potassium extraction and the formation of $Mn_7O_{13}\cdot 5H_2O$ phase, whereas SEM revealed that L-KMO's microstructure is more open and rougher than that of its KMO counterpart. When evaluated as a cathode material for AZIB, L-KMO delivers a high specific capacity of up to 347 mAh g^{-1} at 50 mA g^{-1} current density, with a Coulombic efficiency over 97% throughout cycling. These results demonstrate a simple and scalable approach for developing efficient AZIB cathodes. Future work will focus on optimizing the acid-leaching process for large-scale production and assessing the chemical and electrochemical stability of the produced cathodes under practical operating conditions.

References

[1] B. Tang, L. Shan, S. Liang, J. Zhou, Issues and opportunities facing aqueous zinc-ion batteries, Energy Environ Sci 12 (2019) 3288–3304. https://doi.org/10.1039/C9EE02526J

[2] G. Zampardi, F. La Mantia, Open challenges and good experimental practices in the research field of aqueous Zn-ion batteries, Nature Communications 2022 13:1 13 (2022) 1–5. https://doi.org/10.1038/s41467-022-28381-x

[3] K. Zhu, W. Yang, Vanadium-Based Cathodes for Aqueous Zinc-Ion Batteries: Mechanisms, Challenges, and Strategies, Acc Chem Res 57 (2024) 2887–2900. https://doi.org/10.1021/ACS.ACCOUNTS.4C00484

[4] R. Ajay Rakkesh, S. Shalini, S. Tharani, D. Durgalakshmi, S. Balakumar, Possibilities and challenges of cathode materials for Zn-ion batteries, Energy Advances 3 (2024) 676–688. https://doi.org/10.1039/D3YA00638G

[5] P. Guo, S. Ouyang, H. Jiang, J. Li, H. Zhu, Y. Wang, Application of metal organic frameworks (MOFs) and their derivatives in the cathode materials of aqueous zinc-ion batteries, J Mater Chem C Mater 12 (2024) 18591–18608. https://doi.org/10.1039/D4TC03273J

[6] B. Zhang, P. Dong, S. Yuan, Y. Zhang, Y. Zhang, Y. Wang, Manganese-Based Oxide Cathode Materials for Aqueous Zinc-Ion Batteries: Materials, Mechanism, Challenges, and Strategies, Chem & Bio Engineering 1 (2024) 113–132. https://doi.org/10.1021/CBE.3C00120

[7] M. Karbak, M. Baazizi, S. Sayah, C. Autret-Lambert, Y. Tison, H. Martinez, T. Chafik, F. Ghamouss, Unraveling high-performance oxygen-deficient amorphous manganese oxide as the cathode for advanced zinc ion batteries, J Mater Chem A Mater 11 (2023) 2634–2640. https://doi.org/10.1039/D2TA07838D

[8] C. Wang, M. Wang, Z. He, L. Liu, Y. Huang, Rechargeable Aqueous Zinc–Manganese Dioxide/Graphene Batteries with High Rate Capability and Large Capacity, ACS Appl Energy Mater 3 (2020) 1742–1748. https://doi.org/10.1021/ACSAEM.9B02220

[9] F. Jing, J. Pei, Y. Zhou, Y. Shang, S. Yao, S. Liu, G. Chen, High-performance reversible aqueous Zinc-Ion battery based on Zn2+ pre-intercalation alpha-manganese dioxide nanowires/carbon nanotubes, J Colloid Interface Sci 609 (2022) 557–565. https://doi.org/10.1016/J.JCIS.2021.11.064

[10] S. Ding, M. Zhang, R. Qin, J. Fang, H. Ren, H. Yi, L. Liu, W. Zhao, Y. Li, L. Yao, S. Li, Q. Zhao, F. Pan, Oxygen-Deficient β-MnO2@Graphene Oxide Cathode for High-Rate and Long-Life Aqueous Zinc Ion Batteries, Nano-Micro Letters 2021 13:1 13 (2021) 173-. https://doi.org/10.1007/S40820-021-00691-7

[11] W. Chen, X. Zhan, B. Luo, Z. Ou, P.C. Shih, L. Yao, S. Pidaparthy, A. Patra, H. An, P. V. Braun, R.M. Stephens, H. Yang, J.M. Zuo, Q. Chen, Effects of Particle Size on Mg2+ Ion Intercalation into λ-MnO2 Cathode Materials, Nano Lett 19 (2019) 4712–4720. https://doi.org/10.1021/ACS.NANOLETT.9B01780

[12] N. Liu, M. K., J. Pan, Y. Hu, Y. Sun, X. Liu, A Facile Preparation of λ-MnO2 as Cathode Material for High-Performance Zinc-Manganese Redox Flow Battery, J Electrochem Soc 167 (2020) 040517. https://doi.org/10.1149/1945-7111/AB75C2

[13] H. Afaryate, M. Karbak, M. Kerroumi, M. Aqil, H. Martinez, B. Manoun, Y. Tamraoui, F. Ghamouss, Exploring the synthesis of spinel-type manganese oxide by acid leaching for zinc-ion battery applications, Chemical Engineering Journal 522 (2025) 167548. https://doi.org/10.1016/J.CEJ.2025.167548

[14] S. Ching, D.J. Petrovay, M.L. Jorgensen, S.L. Suib, Sol−Gel Synthesis of Layered Birnessite-Type Manganese Oxides, Inorg Chem 36 (1997) 883–890. https://doi.org/10.1021/IC961088D

[15] Y. Jiao, L. Kang, J. Berry-Gair, K. McColl, J. Li, H. Dong, H. Jiang, R. Wang, F. Corà, D.J.L. Brett, G. He, I.P. Parkin, Enabling stable MnO2 matrix for aqueous zinc-ion battery cathodes, J Mater Chem A Mater 8 (2020) 22075–22082. https://doi.org/10.1039/D0TA08638J

[16] L. Luo, M. Yuan, T. Xie, Q. Chen, Nanoscale assembly and mechanism of K-Birnessite/GOs composite, Results Phys 7 (2017) 3955–3961. https://doi.org/10.1016/J.RINP.2017.10.019

[17] M. Kerroumi, M. Karbak, H. Afaryate, A. El-Bchiri, M. Aqil, B. Manoun, Y. Tamraoui, H. Girault, F. Ghamouss, Unveiling electrochemical insights of lithium manganese oxide cathodes from manganese ore for enhanced lithium-ion battery performance, Electrochim Acta 509 (2025) 145286. https://doi.org/10.1016/J.ELECTACTA.2024.145286

[18] P.E. Saranya, S. Selladurai, Efficient electrochemical performance of ZnMn2O4 nanoparticles with rGO nanosheets for electrodes in supercapacitor applications, Journal of Materials Science: Materials in Electronics 2017 29:4 29 (2017) 3326–3339. https://doi.org/10.1007/S10854-017-8268-5

[19] L. Wang, K.W. Huang, J. Chen, J. Zheng, Ultralong cycle stability of aqueous zinc-ion batteries with zinc vanadium oxide cathodes, Sci Adv 5 (2019). https://doi.org/10.1126/SCIADV.AAX4279;PAGE:STRING:ARTICLE/CHAPTER

[20] W. Xu, Y. Wang, Recent Progress on Zinc-Ion Rechargeable Batteries, Nano-Micro Letters 2019 11:1 11 (2019) 1–30. https://doi.org/10.1007/S40820-019-0322-9